Fourth International Conference on Sustainable Construction Materials and Technologies
http://www.claisse.info/Proceedings.htm

SCMT4
Las Vegas, USA, August 7-11, 2016

Modeling and Measuring Chloride Ingress into Cracked Mortar

Scott Z. Jones*[1a], Jeffrey M. Davis[2], John L. Molloy[3a], John R. Sieber[3b], and Dale P. Bentz[1b]

*[1]National Institute of Standards and Technology, Materials and Structural Systems Division, US, [*1a]Email: <scott.jones@nist.gov>, [1b]Email: <dale.bentz@nist.gov>*

[2]PNDetector GmbH, DE, [2]Email: <jeff.davis@pndetector.de>

[3]National Institute of Standards and Technology, Chemical Sciences Division, US, [3a]Email: < john.molloy@nist.gov>, [3b]Email: <john.sieber@nist.gov>.

ABSTRACT

Chloride ingress into reinforced concrete structures is a cause of corrosion of steel embedded into concrete. To aid in the prediction of concrete service life, a chloride ingress model that includes the effects of physical absorption to and chemical reaction with the cement matrix as well as time-dependent diffusivity is derived by a mass balance and solved by the finite element method. This model is validated through an experimental program where the chloride concentration around cracked specimens is measured using microbeam X-ray fluorescence spectrometry (µXRF). Reinforced mortar beams are cast and cracked by three-point bending. The samples are submerged in a chloride solution for time periods between 7 d and 21 d. The data collected from the µXRF scans is processed using a support vector machine (SVM) algorithm to identify the cement paste matrix. The chloride counts in the matrix are processed by a generalized additive model (GAM) to interpolate the counts over the scan domain. The data is calibrated using standards with known chloride concentrations and the results are compared to the finite element based model which shows good agreement between experiments and modeling. This demonstrates the necessity and usefulness of developing a chloride ingress model that accounts for both chloride ion and cement matrix interactions, the time-dependent behavior of the apparent diffusivity, and crack geometry.

INTRODUCTION

Service life prediction models vary in complexity, from the use of empirical relations for time dependent diffusivity in Fick's Second Law (Vu et al., 2013) to models that capture the effects of water absorption, relative humidity within the pore structure, and ion to ion interactions (Samson et al., 2005). These models do not capture the effects of a crack that may be present in the structure's concrete. The presence of a crack has been shown to dramatically increase the local chloride concentration, at a given cover depth, by providing a preferential pathway for chloride ions to move into the concrete matrix (Bentz et al., 2013, Şahmaran and Yaman, 2008). The presence of cracks in the concrete cover must be accounted for if service life models are to represent conditions to which a concrete structure is exposed (Bentz et al., 2014, Lu et. al. 2013). In this study, reinforced mortar beams are cracked under three-point bending and then submerged in a solution of 1 mol/L sodium chloride (NaCl). After periods between 7 d and 21 d, the specimens are removed from the solution

and cut perpendicular to the crack. Chloride concentration was determined using microbeam X-ray fluorescence spectrometry (μXRF). A support vector machine (SVM) algorithm was used to identify the cement paste and a generalized additive model (GAM) was used to interpolate the chloride counts over the scan domain. The results are compared to a mass balance model and show good agreement. The selection of the effective chloride binding reaction rate affects the simulation results by shifting the magnitude of the chloride concentration at a given depth. Selection of this parameter is important to service life calculations and is likely dependent on the physical and chemical properties of the cementitious system.

The model described in this work is an extension of the work of Bentz et al., 2014, Lu et. al. 2013, and Jones et al. 2015, where experimental measurements of the time-dependent transport properties of mortars are used as inputs to the model. Chloride measurements made at 25 μm intervals allow for a spatial resolution that is suitable for verifying modeling assumptions outlined in Bentz et al., 2014, Lu et. al. 2013, and Jones et al. 2015; specifically, the treatment of the transport properties around a crack can be assessed with this measurement technique.

MATERIALS AND METHODS

Cracked Mortar Beams. Mortar beams, measuring 4 cm x 4 cm x 16 cm were created with type I Portland cement. The cement used was Cement and Concrete Reference Laboratory (CCRL) material number 192 (January 2014). Chemical analyses were obtained from the consensus values available from CCRL (www.ccrl.us). Two water-to-cement ratios were studied, *w/c* = 0.4 and 0.5. These *w/c* values produce mortars with different effective diffusivities. Details of the mixture proportions using a blend of four sands are given in Table 1. All materials were weighed to the nearest 0.1 g.

Table 1. Mixture proportions in kg of material per total volume of materials (m^3)

	w/c = 0.4	*w/c* = 0.5
Cement	637.1	637.1
Water	254.8	318.6
ASTM F95 sand	357.1	357.1
ASTM Graded sand	271.4	271.4
ASTM 20-30 sand	271.4	271.4
ASTM GS-16 sand	528.5	528.5

A single section of threaded stainless steel rod was placed at the center of each beam and served as reinforcement of the specimen. In each beam, a crack was created by loading the specimen in 3-point bending after 7 d sealed curing. When the specimens reached an age of 28 d, they were removed from the curing chamber and placed in a 1 mol/L NaCl solution at 23 °C, until they were removed for μXRF analysis. After removal from the chloride solution, specimens were placed in a freezer at -10 °C at atmospheric pressure to slow subsequent diffusion. Samples were prepared for μXRF analysis by sectioning the beams into thirds and cutting perpendicular to the crack with a diamond saw. Cuts were made in 200-proof ethanol to limit the disruption of chloride ions. The surfaces to be scanned were polished with 120 grit SiC abrasive paper and ethanol.

Microbeam X-ray Fluorescence Spectrometry

μXRF settings and configuration. Chloride concentrations were determined from measurements made using a microbeam X-ray fluorescence spectrometer with a Rh X-ray source and a 25 μm thick Al primary beam filter. The X-ray tube voltage and current were set to 40 kV and 1000 μA, respectively. The nominal beam spot size was 50 μm, and the area measured was approximately 14

mm by 20 mm, centered on the crack. Measurements were made at 25 µm intervals, corresponding to an approximately half X-ray beam overlap, in a raster pattern. Spectra were acquired for 400 ms per location with the detector pulse shaping time set to 12.8 µs. X-Ray counts for Cl and other elements in the cement matrix were obtained from each spectrum by fitting peaks after background calculations and subtraction.

Calibration of µXRF data. Calibration of µXRF data was achieved by preparing mortar specimens, composed of the same materials as the test specimens and in the same proportions, with known additions of chloride ions. The data output from the µXRF is in the form of a spectrum of counts *vs.* electron volts (eV) at each pixel. The counts in the range of 2.40 keV to 3.00 keV (corresponding to Cl Kα and Cl Kβ lines) at each pixel are fit to a log-normal distribution. The mean is computed and plotted versus the added chloride concentration with respect to total mortar volume. A simple linear model is assumed ($Y = \beta_1 X + \beta_0$), and the added chloride concentration is regressed onto the expected values of the counts. Initial regression analysis produced a β_0 = - 27 mol/m^3 and a standard error, SE = 32.5 mol/m^3. A hypothesis test suggested that β_0 is not statistically different from zero. The regression analysis was performed again with $\beta_0 = 0$ to produce the parameters shown in Table 2. Akaike's Information Criterion (AIC) suggests that the linear model with the intercept constrained to zero is best suited to predict the expected value of concentration (Wood, 2001, p.31). The estimate of β_1 in Table 2 has a low standard error and a *t*-statistic greater than the degrees of freedom (DOF) (*n* - 1), where *n* is number of samples. This indicates a relationship between the chloride concentration and the expected value of the counts, and it is estimated by the model $Y = \beta_1 X$.

Table 2. Coefficient estimates of linear model $Y = \beta_1 X$.

		Est. (mol/m^{3}count)	Std. Error (mol/m^{3}count)	*t*-statistic	*p*-value	DoF
w/c = 0.4	β_1	0.0378	2.4E-03	15.74	2.66E-07	8
w/c = 0.5	β_1	0.0356	2.3E-03	15.74	2.66E-07	8

Support Vector Machine and Generalized Additive Model. µXRF data was collected by rastering the sample under a stationary X-ray beam in an array with equally spaced points of 25 µm. The data of interest is the chloride ion concentration in the cement paste. Pixels from the coarse and fine aggregates, epoxy, as well as the interfacial transition zone around the aggregates were not included in the concentration model. Since cement paste contains Si, Ca and varying amounts of Cl, simple linear combination models are not sufficient to adequately segment the data. Further, the case of an analysis point that contains both cement and aggregate needed to be addressed. A training data set was collected from a mortar sample, of the same mix design, that contained no added chlorides (CCRL 192 contains 0.031 % by mass Cl) and was scanned under the same scan settings as the test specimens.

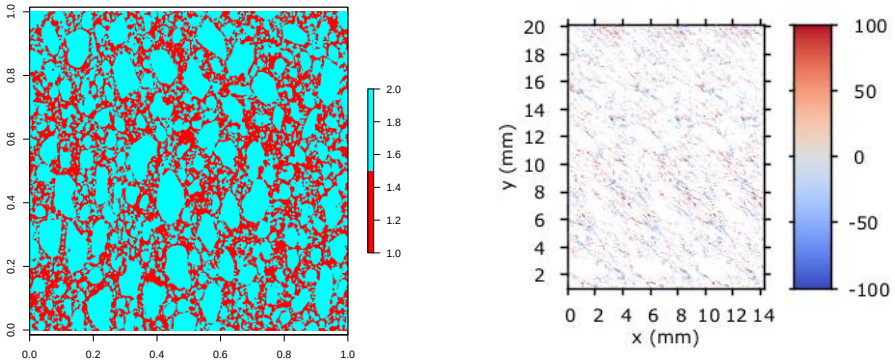

(a) Phase Identification by SVM (b) Residuals of GAM

Figure 1. (a) Training data set produced by the SVM. The red indicates paste while the teal indicates aggregates. (b) Residuals of the GAM fit for the 2000 mol/m^3 Cl$^-$ standard. The scale limits are set to +/- 100 mol/m^3 to improve visualization of residual distribution.

This data set was used to train a support vector machine (SVM) to distinguish between two phases, aggregates and paste. The SVM does not rely on a linear combination of elemental compositions or on a defined count range. Rather, the model is able to separate out the data purely from the resulting X-ray spectrum, and, as a result, it is very efficient for processing the data and extracting the phase information. The resulting phase identification is given in Figure 1a, which shows the aggregates in cyan and the paste in red. The model can be adjusted to exclude the interfacial transition zones around the aggregates, but it was not able to account for aggregates that were smaller than the beam size of 50 μm. The SVM was used to produce a map of chloride counts only in the regions that contain paste. For this study, a generalized additive model (GAM), Equation 1, is used to interpolate the count over the domain.

$$\text{counts} = s(x) + s(y) + s(x,y) \tag{1}$$

The functions s(x), s(y), s(x,y) are smoothing splines which serve as the basis for the GAM (James et al., 2013, p.282, Wood, 2011, p.121). A square root link function is used, and the number of knots required for the smoothing splines is determined by 3-fold cross validation. The residuals in Figure 1b are uniformly distributed about the domain indicating the probability of obtaining a certain error at a given point has a normal distribution. The result is a smooth representation of the chloride counts in the specimen.

Mortar Transport

To determine the transport properties required for simulations, several mortar mixtures were made for analyses of their pore solution resistivity, bulk resistivity, and chloride binding capacity. The time-dependent value of the mortar diffusivity can be estimated by monitoring the pore solution resistivity and bulk resistivity over time. Pore solution was extracted from mortar cylinders by the procedure described in (Barneyback and Diamond, 1981). The resistivity was measured by filtering the extracted pore solution through a 0.2 μm filter and using a resistivity cell, calibrated with KCl solutions of known conductivity (ed. Settle, 1997), to measure electrical impedance. The values were fit to the function shown in Equation 2. The assumed functional form of the diffusivity is given in Equation 3, where D(t) is found using Equation 4. Pore solution resistivity and mortar diffusivity coefficients are given in Table 3 with the corresponding plots given in Figure 2.

$$\rho_{ps} = C + A \cdot t^{b} \tag{2}$$

$$D(t) = D_{\infty} + D_i \cdot t^{m} + D_{ib} \cdot t^{l} \tag{3}$$

$$\rho_c/\rho_{ps} = D_0/D(t) \tag{4}$$

Table 3. Curve fit parameters for pore solution resistivity and diffusivity of mortars

Parameter		Value	Std. Error
w/c = 0.4	C	0.0972 Ω-m	0.0034 Ω-m
	A	0.7805 Ω-m/s	0.0501 Ω-m/s
	b	-0.8782	0.0589
w/c = 0.5	C	0.1027 Ω-m	0.0143
	A	0.5022 Ω-m/s	0.0286
	b	-0.4193	0.0575

	Value	Std. Error
D_∞	2.143E-12 m^2/s	1.92E-13 m^2/s
D_i	6.910E-09 m^2/s^2	2.09E-10 m^2/s^2
D_{ib}	9.932E-11 m^2/s^2	3.52E-12 m^2/s^2
m	-2.467E+00	2.1E-02
l	-5.37E-01	1.2E-02
D_∞	7.821E-12 m^2/s	4.20E-13 m^2/s
D_i	3.487E-09 m^2/s^2	2.54E-10 m^2/s^2
D_{ib}	4.868E-10 m^2/s^2	6.95E-11 m^2/s^2
m	-2.113E+00	9.7E-02
l	-8.424E-01	3.8E-02

To improve the numerical stability of the finite element (FE) model, the data in Figures 2a and 2b were fit to Equations 2 and 3 using a non-linear least-squares regression routine. Equation 3 is used to determine the bulk diffusivity at a given time point. The very early age diffusivity (t < 3.5 h for *w/c* = 0.4 and t < 5 h for *w/c* = 0.5) is assumed to be constant as the changes in pore solution and bulk resistivity are relatively small over these time periods. The parameters used in the finite element model are given in Table 3. The absolute value of m in equation 3, for both *w/c* = 0.4 and 0.5 is greater than 1. Bentz et al., 2000, mention that a value greater than 1 cannot be used with an analytical solution, but Equation 3 has been employed for a numerical approach. The curve of the fitted diffusivity values is given in Figure 2b, which shows the proper decrease in diffusivity with time in the time period of interest. An important component to modeling chloride ion concentration is the effects of physical absorption to and chemical reaction with the cement matrix. This is accomplished by a procedure given by Luping and Nilsson, 1993. After 28 d of sealed curing, the mortar was ground to a powder and passed through a sieve with a 1680 µm opening. The chlorides bound to the cement paste per kg of cement are given in Figure 3 for both *w/c* = 0.4 and *w/c* = 0.5. Table 4 gives the coefficients of a Langmuir isotherm determined from a non-linear regression.

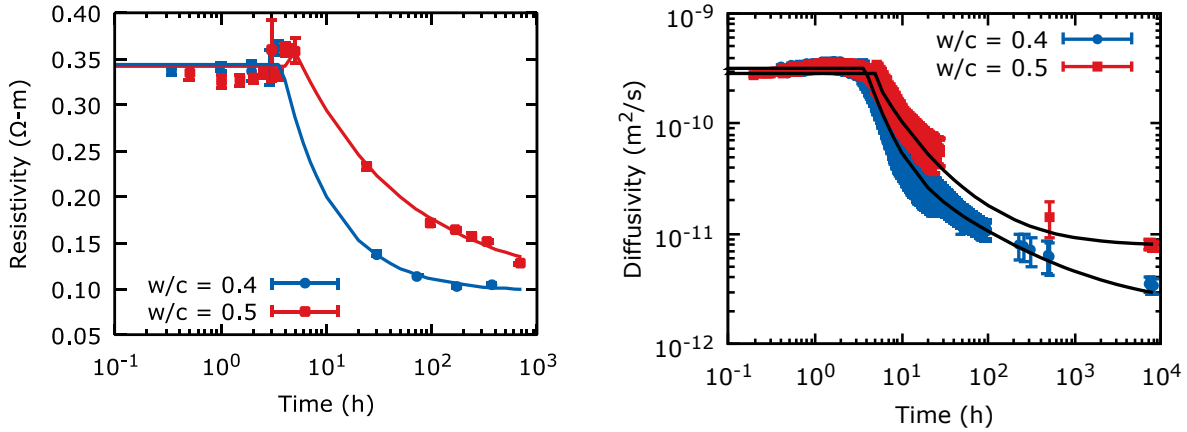

(a) Pore Solution Resistivity (b) Mortar Diffusivity (c)

Figure 2. (a) Plot of measured pore solution resistivity. (b) Plot of the estimated diffusivity of the mortar determined from the non-linear regression in (a) and the measured mortar resistivity. The solid lines in (a) and (b) are the curves resulting from non-linear regression. Error bars represent the 95 % confidence interval of the measured data.

Table 4. Parameters determined from non-linear least squares regression of Langmuir isotherms of chloride binding measurements.

Isotherm		*w/c* = 0.4		*w/c* = 0.5	
		Value	Std. Error	Value	Std. Error
Langmuir	α	4.01E-02	6.4E-03	4.890E-02	2.2E-04
	β	1.10E-03	4.0E-04	2.54E-03	3.6E-04

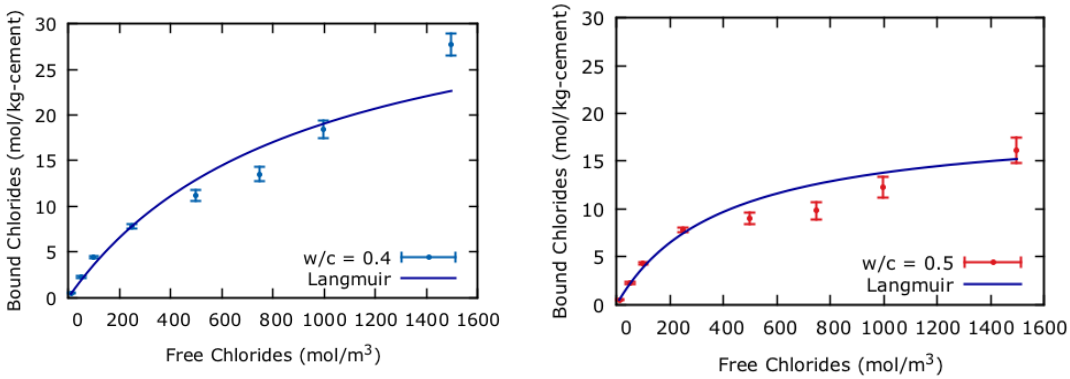

(a) *w/c* = 0.4 (b) *w/c* = 0.5

(c)

Figure 3. Chloride binding isotherms for (a) *w/c* = 0.4 mortar and (b) *w/c* = 0.5 mortar. Bound chlorides are plotted as the number of moles of chloride ions bound per kg of cement in the mixture. Chloride binding in these plots is assumed to be the sum of physically absorbed chloride ions and ions consumed in Friedel's salt formation. Error bars represent the 95 % confidence interval.

Mass Balance Model

Transport of chloride ions through the paste matrix (cement and water) is derived from a mass balance on an infinitesimal volume of the domain of interest, shown schematically in three dimensions in Figure 4a. Formulating the governing equations in the paste is equivalent to assuming that the aggregates do not absorb or transport chloride ions through them. Within the paste, chloride transport is assumed to occur through the water saturated pore structure. The flux across a face of the control volume is $\mathbf{j_i} = D_{con}(t)\nabla C_{f\text{-}pore} = \varepsilon_p D_{con}(t)\nabla C_f$ where $C_{f\text{-}pore}$ is expressed in terms of water accessible pore volume and C_f is expressed in terms of paste volume. The time rate of change of the chloride concentration in the paste volume is equal to the sum of the flux going into the volume minus the flux leaving the volume plus accumulations of chlorides inside the volume. This is expressed mathematically in Equation 5 where Fick's Law is used to relate the flux to the free chloride concentration (C_f). In Equation 5, the binding of free chlorides to the mortar matrix is modeled as a first order reaction with reaction rate k. The water accessible porosity of the paste is ϵ_p. The change in concentration of bound chlorides (C_{bound}) is described by Equation 6, where ($C_{bound\text{-}eqbm}$) is the equilibrium concentration of bound chlorides.

$$\frac{\partial C_f}{\partial t} = \nabla \cdot \left(\epsilon_p D_{con}(t) \nabla C_f\right) + k\left(C_{bound} - C_{bound-eqbm}\right) \quad (5)$$

$$\frac{dC_{bound}}{dt} = \epsilon_p k\left(C_{bound-eqbm} - C_{bound}\right) \quad (6)$$

$$C_{bound-eqbm} = \alpha C_f/(1 + \beta C_f) \quad (7)$$

The relationship between the free chloride concentration and the concentration of chlorides that will react with the cement paste, at equilibrium, is described by the Langmuir isotherm, Equation 7. Two domains are used in the simulations. Figure 4b shows the control, un-cracked case while Figure 4c, shows a representation of a cracked case where the crack geometry is imported into the model from the μXRF images.

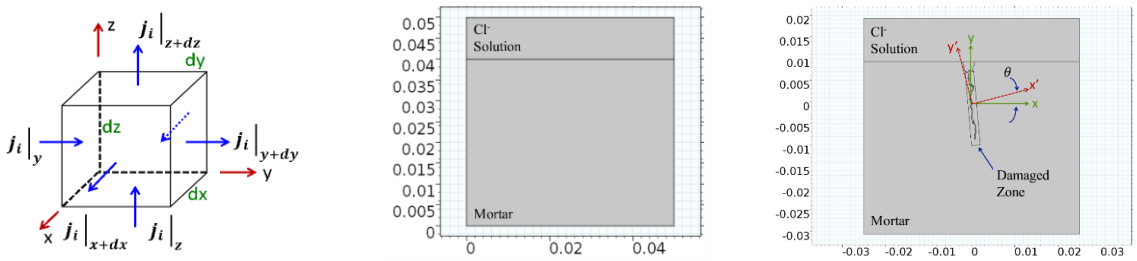

(a) Control Volume (b) Un-cracked Case (c) Cracked Case

Figure 4. (a) Schematic representation of the infinitesimal control volume, (b) the domain representing the un-cracked case, and (c) cracked case (units: m).

RESULTS AND DISCUSSION

Control Case – No Crack. A domain without a crack is modeled as a control case. This scenario is considered the "best case" for protection of the rebar from corrosion and serves as a reference for the ability of the model to predict chloride ion concentration. Figures 5a-b and Figures 5c-d show results of a specimen exposed to a 1 mol/L NaCl solution for 7 d and 15 d, respectively. Figure 5a shows the results of the μXRF scan and Figure 5b shows the results along three lines, from y = L to y = 0, across the domain. The shaded region of the plot in Figure 5b is the measurement uncertainty at a 95 % CI, as determined by the procedure described in JCGM 101:2008. Figure 5 shows good agreement between the model and the measured results of the μXRF scans. In Figure 5b, the model is within the measurement uncertainty. A similar result is observed in Figures 6a-d. The model agrees well with the μXRF data near the top surface in Figure 6b but underestimates the measured values as the distance increases. This may be a result of the calibration procedure. In Figure 6d, there appears to be an inflection point in the measured data at 4 mm. Upon closer inspection of the sample, there appears to be a void just below the surface which will affect the counts. However, the model does follow the general trend of the measured data. The results in Figure 5a-d (and 6a-d) exhibit good agreement between the model and measured data. The chloride binding reaction rate, k, is assumed to be an effective reaction rate which includes both physical absorption of chloride ions onto calcium silicate hydrate (C-S-H), as well as the formation of reaction products such as Friedel's salts. In previous modeling studies, the chloride binding reaction rate was assumed to be 3.0E-07 1/s (Jones et al., 2015, Bentz et al., 2013). The concentration in the storage solution was measured at intervals of approximately 24 h for the first 3 d and then approximately 7 d thereafter. It was observed that the chloride binding experiments reached their equilibrium states within 2 d, corresponding to a reaction rate of approximately 5.7E-06 1/s. Since the time to equilibrium of the chloride binding experiments is a function of the particle size of the ground mortar, it is likely that this effective reaction rate would be much slower in a system where chlorides are diffusing though a pore structure, as the surface area available for chloride binding would be much lower.

To study the influence of k, the simulations were run with k = 1.0 s^{-1}, 3.0E-07 s^{-1}, and 0 s^{-1}. Figures 5b and 5d (and Figure 6b and 6d) demonstrate the influence of the effective chloride binding rate on the simulation results. Simulation results indicate that the model is not sensitive to the reaction rate so long as the time steps taken by the solver are long enough to allow for the binding reaction to reach equilibrium. The μXRF results suggest that chloride binding is happening at a rate closer to the assumed value of 5.7E-06 1/s. When the reaction rate is reduced, the influence of the chloride binding is reduced – $k \rightarrow 0$ removes the chloride binding term from Equation 5. This result indicates the need for a better measurement of chloride binding kinetics and suggests a first-order reaction rate may not be an appropriate approximation. Still, the simulation results are within the measurement uncertainty indicating the simulation may provide a suitable estimation of chloride concentration at a given position and time. Deviation of the

measured values from simulation results may be explained by increased porosity due to leaching of portlandite and decalcification of C-S-H resulting from hydrolysis of the cement paste (Carde and Francois, 1997). This change in the matrix will affect X-ray counts due to changes in grain sizes that are a result of the increased porosity (Jenkins and De Vries, 1975).

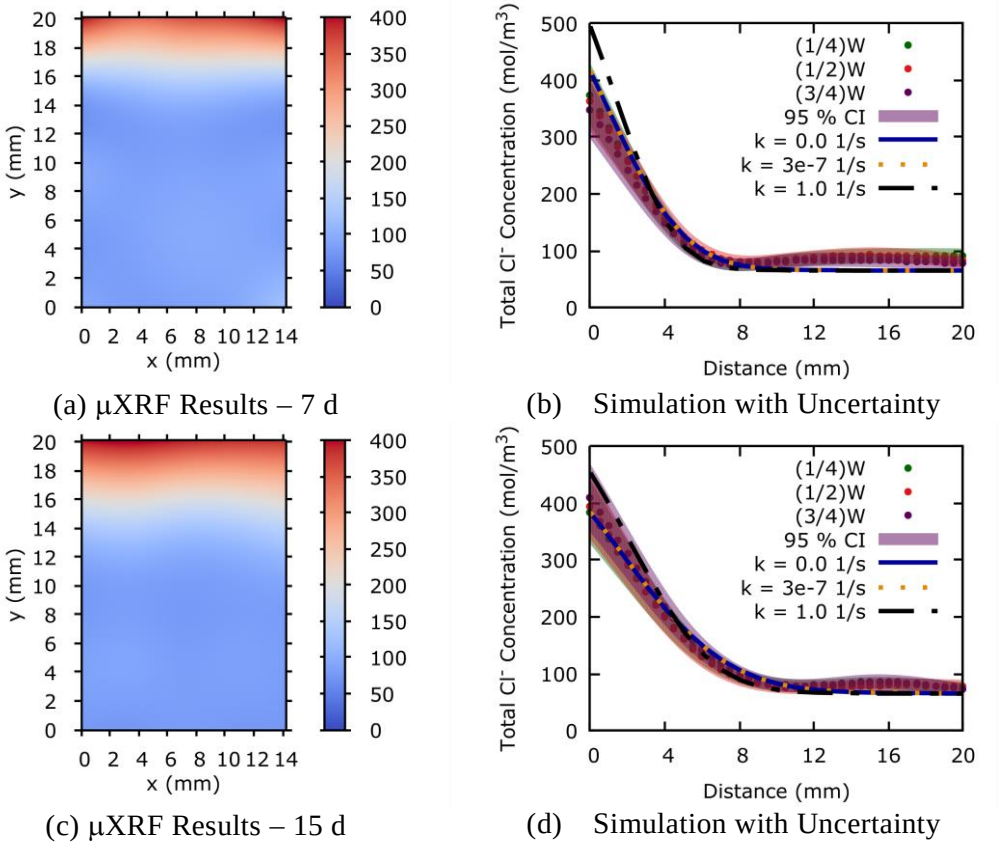

(a) μXRF Results – 7 d (b) Simulation with Uncertainty

(c) μXRF Results – 15 d (d) Simulation with Uncertainty

Figure 5. Total Chloride ion concentration in control specimen of *w/c* = 0.4 at 7 d exposure (a) & (b) and 15 d exposure (c) & (d) as measured by μXRF, (a) & (c), and solution to eq. 5 & 6, (b) & (d). The concentration measured from the top, exposed surface and the measurement uncertainty at a 95 % confidence interval is shown. "W" is the maximum x-direction value. Concentration is expressed in moles per m^3 of mortar.

Saturated Crack Case. Simulations of cracked mortar are performed as in the control case but with a few important modifications to the model. The crack geometry is imported to the FE software by combining the Si and Ca μXRF images, converting them to a binary image, and then adjusting the threshold such that only the crack outline is visible (Figure 4c).

Previous studies attempting to simulate chloride concentration around cracks have assumed that a region around the crack has diffusivity properties that are different from the bulk. Jones et al., 2015 and Bentz et al., 2013 assumed this region to be approximately 4 mm from the crack edge. This assumption was based on experimental evidence reported in Şahmaran and Yaman, 2008 and the chloride maps presented in Figure 7a and Figure 8a support these findings, as the depth of penetration from the crack surface appears to be greater than that from the top, exposed surface. Following the simulation procedures outlined in Jones et al., 2015 and Bentz et al., 2013, the chloride profile for two cracked domains are simulated by solving Equations 5 through 7. The crack in the sample tends to deviate from vertical. To account for this phenomenon, the damaged zone region was rotated around its center point to align with the crack. Since Equation 5 is formulated assuming the principal directions of the flux are in line with the x and y axes, a

rotation is applied to the diffusivity tensor which produces components $D_{xx} = D_{yy} = DF \cdot D(t)\cos(\theta)$ and $D_{xy} = -D_{yx} = -DF \cdot D(t)\sin(\theta)$ where DF is a parameter used to estimate the increase in diffusivity. The parameter DF is thought to be a result of increased porosity around the crack possibly due to micro-cracking. Figure 7a shows the chloride concentration as measured by μXRF and Figure 7c shows the concentration as a function of depth with (1/2)W approximately centered on the crack, where the symbols represent measured results and the lines represent simulation results. The simulation was run with DF = 1, 10, and 20 and the width of the damaged zone = 1 mm (1.5 mm for *w/c* = 0.5). The convergence of the simulation to the μXRF results improved as DF increased to 10 for *w/c* = 0.4 and 20 for *w/c* = 0.5. The simulation results in Figure 7 are shown with DF = 10 and agree well with the measured μXRF results. Increasing DF to 20 produced results that exceeded measured values near the crack tip.

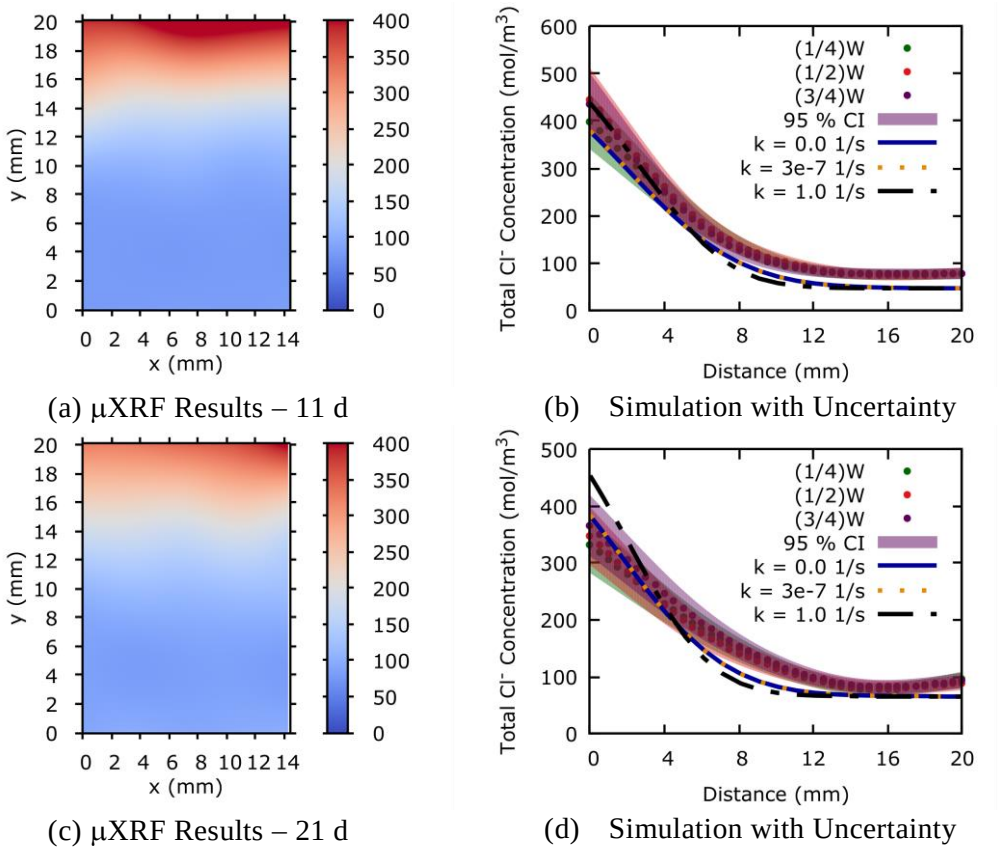

(a) μXRF Results – 11 d (b) Simulation with Uncertainty

(c) μXRF Results – 21 d (d) Simulation with Uncertainty

Figure 6. Total Chloride ion concentration in control specimen of *w/c* = 0.5 at 11 d exposure (a) & (b) and 21 d exposure (c) & (d) as measured by μXRF, (a) & (c), and solution to eq. 5 & 6, (b) & (d). The concentration measured from the top, exposed surface and the measurement uncertainty at a 95 % confidence interval is shown. "W" is the maximum x-direction value. Concentration is expressed in moles per m^3 of mortar.

The model predicts the chloride concentration near the top and bottom of the scanned area but tends to over predict measured chloride concentrations near the middle. The dips in the simulation result from regions where the model results are in the crack domain, which does not bind chlorides. Figure 8 shows the results for a crack in a *w/c* = 0.5 mortar with DF = 20 in a region around the crack. The simulation results in Figure 8 agree well with the μXRF results but do not appear to capture the behavior near the top surface. This is likely due to positional errors introduced into the model when converting the Si and Ca μXRF images into a format that can be

accepted by the model. However, the behavior away from the top surface is in agreement with the μXRF measurements and is therefore a suitable approximation to the observed measurements.

Figures 7 and 8 present a comparison between experimental measurements of chloride concentration and simulation results. Jones et al. 2015, performed a series of simulations, which attempted to model the chloride concentration around rectangular cracks. Based on the work of Şahmaran and Yaman, 2008, a region around the crack was defined to have a diffusivity approximately 20 times the bulk diffusivity.

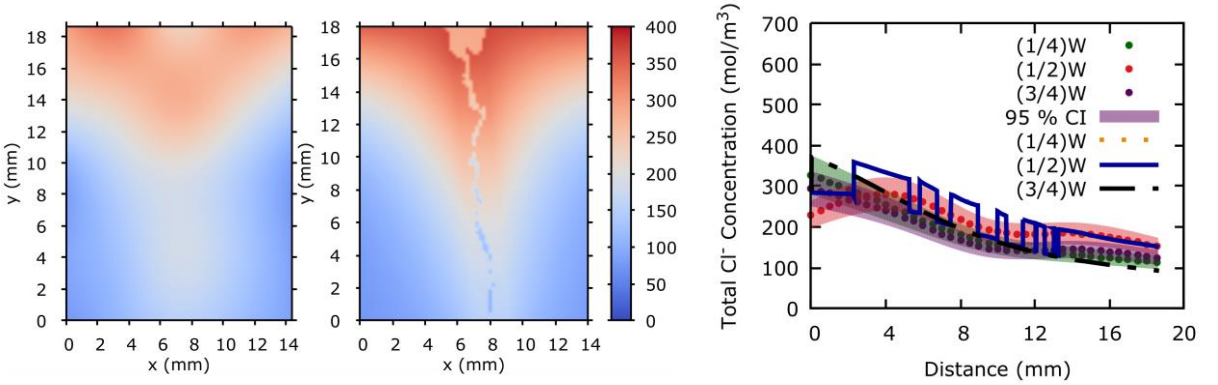

(a) μXRF Results (b) Simulation Results (c) Simulation with Uncertainty

Figure 7. Total Chloride ion concentration in cracked specimen (*w/c* = 0.4 crack at 14 d exposure, DF = 10) as measured by (a) μXRF and (b) & (c) solution to eq. 5 & 6. The concentration measured from the top, exposed surface and the measurement uncertainty at a 95 % confidence interval is shown in (b). "W" is the maximum x-direction value.

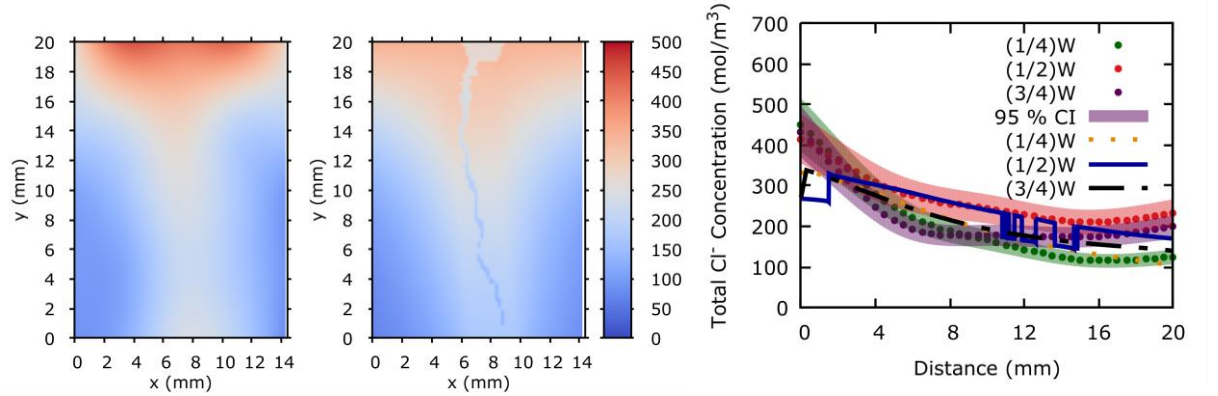

(a) μXRF Results (b) Simulation Results (c) Simulation with Uncertainty

Figure 8. Total Chloride ion concentration in cracked specimen (*w/c* = 0.5 crack at 15 d exposure, DF = 20) as measured by (a) μXRF and (b) & (c) solution to eq. 5 & 6. The concentration measured from the top, exposed surface and the measurement uncertainty at a 95 % confidence interval is shown in (b). "W" is the maximum x-direction value.

Based on the work of Şahmaran and Yaman, 2008, a region around the crack was defined to have a diffusivity approximately 20 times the bulk diffusivity. Chloride concentration measurements were made on the extraction fluid of powdered mortar that was obtained by drilling to known depth. This measurement technique produces an estimate of the diffusivity for the region sampled by the coring bit. With an approximate spatial resolution of 25 μm – it should be noted that the X-ray beam spot size is 50 μm, so in this study, spatial resolution indicates the approximate edge size of one pixel in the data set – the transport properties can be assessed at smaller length scales. With this enhanced measurement technique, Figures 7 and 8 indicate that DF is variable and is dependent on the crack

geometry. The model detailed in this study addresses crack orientation by aligning the principal directions of the diffusivity tensor with the crack. These two factors improved convergence between experimental measurements and simulation results as shown in Figures 7c and 8c.

CONCLUSION

In this study, experimental and modeling procedures are detailed to measure the chloride concentration around a crack created in a reinforced mortar beam. Measurements are made on samples with and without a crack, for *w/c* = 0.4 and *w/c* = 0.5 mortars. Simulation results are within the measurement uncertainty when the uncertainty is derived using a Monte Carlo method for simulating data. Using the FE simulation to conduct a parametric study of the effective chloride binding reaction rate indicates that the value of the parameter can be estimated from the time it takes the chloride binding experiments to reach equilibrium. When a crack is present in the domain of interest, a region around the crack is defined to have a diffusivity 10 or 20 times greater than the bulk mortar, depending on the mortar *w/c*. Orienting this region in the direction of the crack and conducting a parametric study of the DF factor produced results that were within the uncertainty of the μXRF measurements. The results presented in this paper demonstrate the deleterious effect of a crack on the protection capacity of a cementitious cover over a steel bar. The model presented is able to predict chloride concentrations when given the appropriate inputs for the material under investigation. Experimental measurements taken with a spatial resolution of approximately 25 μm over an approximately 14 mm x 20 mm domain allow for model verification at spatial increments suitable for studying the DZ diffusivity. A better prediction of chloride concentration near cracks will improve service life models by moving the model closer to real-world conditions.

REFERENCES

Barneyback Jr., R.S., and Diamond, S. (1981) Expression and Analysis of Pore Fluids from Hardened

Cement Pastes and Mortars. *Cement and Concrete Research*. 11 (2). p. 279-285.

Bentz, D.P., Feng, X., & Hooton, R.D. (2000) Time-dependent diffusivities: possible misinterpretations due to spatial dependence. *Testing and Modeling the Chloride Ingress into Concrete. Proceedings. 2nd International RILEM Workshop.* September 11-12, Paris, France, p. 225-233.

Bentz, D.P., Garboczi, E.J., Lu, Y., Martys, N., Sakulich, A.R., & Weiss, W.J. (2013) Modeling of the

influence of transverse cracking on chloride penetration into concrete. *Cement and Concrete Composites.* 38. p.65-47.

Bentz, D.P., Guthrie, W.S., Jones, S.Z., and Martys, N.S. (2014) Predicting Service Life of Steel

Reinforced Concrete Exposed to Chlorides: A discussion of real-world considerations for effective modeling, *Concrete International*. 36 (9). p. 55-64.

Carde, C., and Francois, R. (1997) Effect of ITZ leaching on durability of cement-based materials.

Cement and Concrete Research. 27(7). p. 971-978.

James, G. et al. (2013) *An Introduction to Statistical Learning with Applications in R.* NY: Springer.

JCGM 101:2008; *Evaluation of measurement data – Supplement 1 to the "Guide to the expression of*

uncertainty in measurement" – Propagation of distributions using a Monte Carlo method; Joint Committee for Guides in Metrology (JCGM) (2008).

Jenkins, R. and De Vries, J.L. (1975) *Practical X-Ray Spectrometry*. New York: Springer-Verlag p. 118.

Jones, S.Z., Martys, N.S., Lu Y., Bentz, D.P. (2015) Simulation Studies of Methods to Delay Corrosion and Increase Service Life for Cracked Concrete Exposed to Chlorides. *Cement and Concrete Composites* 58 p.59-69.

Lu, Y., Garboczi, E.J., Bentz, D.P., and Davis, J.M., Modeling Chloride Transport in Cracked Concrete: A 3-D Image-Based Microstructure Simulation, *Proceedings of the 2012 COMSOL conference, Boston*, MA, 2012.

Luping, T., Nilsson, L.O., (1993) Chloride binding capacity and binding isotherms of OPC pastes and Mortars. *Cement and Concrete Research* 23 (2). p.247-253.

Mills, R. & Lobo, V.M.M. (1989) Self-Diffusion in Electrolyte Solutions. New York: Springer.

Şahmaran, M., & Yaman, İ. Ö., (2008) Influence of transverse crack width on reinforcement corrosion initiation and propagation in mortar beams. *Canadian Journal of Civil Engineering* 35 (3). p.236-245.

Samson, E., Marchand, J., Snyder, K.A., & Beaudoin, J.J. (2005) Modeling Ion and Fluid Transport in Unsaturated Cement Systems in Isothermal Conditions. *Cement and Concrete Research* 35 (1). p.141-153.

Settle, F (ed.) 1997, *Handbook of Instrumental Techniques for Analytical Chemistry*, Prentice Hall, New Jersey, p.760.

Vu, H.Q., Stitmaannaithum, B., & Sugiyama T. (2013) Prediction of Chloride Profile at Crack Location in Reinforced Concrete Under Flexural Loading. *ASEAN Engineering Journal Part C.* 2 (1).

Wood, S.N. (2011) *Generalized Additive Models An Introduction with R.* New York: CRC Press.